Design of Nanoscale Hybrid Insulator-metal-insulator Plasmonic Waveguide

Pintu Kumar (pintu.ec15@nitp.ac.in)
NIT Patna: National Institute of Technology Patna https://orcid.org/0000-0002-7397-758X
D. K. Singh
National Institute of Technology Patna
Rakesh Ranjan
NIT Patna: National Institute of Technology Patna

Research Article

Keywords: Surface wave, Hybrid plasmonic waveguide, Propagation loss, Crosstalk, Photonic integrated circuits

Posted Date: March 5th, 2021

DOI: https://doi.org/10.21203/rs.3.rs-252702/v1

Version of Record: A version of this preprint was published at Silicon on April 28th, 2021. See the published version at https://doi.org/10.1007/s12633-021-01111-6.

Design of nanoscale hybrid insulator-metal-insulator plasmonic waveguide

Pintu Kumar, D. K. Singh, and Rakesh Ranjan
OFC and Photonics Research lab,
Department of Electronics and Communication Engineering,
National Institute of Technology Patna, India.
*E-mail: pintu.ec15@nitp.ac.in

Abstract. Optical properties of the fundamental hybrid mode of hybrid insulator-metal-insulator plasmonic waveguide (HIMIPW), consists of insulator-metal-insulator sandwiched between two dielectric waveguides, have been investigated to achieve the relatively high propagation length and large normalized intensity at 1.55 µm working wavelength. The main aim of the current work is to settle the issues of high power loss and size of waveguide dimension. The optimum waveguide dimension of 0.2 µm × 0.02 µm has been obtained propagation length around 289.26 µm. The normalized intensity in the low-index region of the HIMIPW has been achieved around 67.50μm^{-2}, due to the electric field enhancement in this region. It is beneficial for the design of bio-sensing, optical manipulations, etc. The electric field intensity has been attained highest values at wavelength 1.55 µm for the optimum dimension of the HIMIPW (w = 0.2 µm, t_h = 0.2 µm, and t_l = 0.02 µm), due to highly localized surface plasmon resonance at the metal-dielectric interfaces. The investigation of the coupling length between the two identical parallel HIMIPWs with a separation distance has been done. Further to improve the coupling length, a metallic strip has been inserted between them, keeping the separation distance unchanged. The higher coupling length leads to lower crosstalk between two parallel hybrid plasmonic waveguides, which can be highly useful to achieve the larger integration over the photonic chip.

Keywords: Surface wave, Hybrid plasmonic waveguide, Propagation loss, Crosstalk, Photonic integrated circuits.

1 Introduction

Nowadays, the technology requires higher bandwidth communication services, such as high quality-video/image transfer, cloud computing, etc., which can be achieved efficiently by the systems/networks based on optical technology. For the optical technologies, the optical waveguides are one of the essential devices. In order to achieve the high optical integrations, optical devices have to be improved with miniaturization of size and smaller losses. The propagation loss in the photonic/dielectric waveguides are almost negligible, but, it suffers from diffraction limit [1, 2]. Due to the coupling between photons and free electron density oscillation of the metal, the localized surface plasmon resonance are excited at the surface of metal-dielectric interfaces produces extremely localized enrichment and it can be offer tight light confinement and guidance of electromagnetic waves (EWs) below the diffraction limit [3-7], and hence, resolves the issue of diffraction limit. Plasmonic mechanism allows the optical signal/data propagate through the true-nano scale regions (<100 nm) [8-12], but suffers from high propagation losses due to the presence of metal. The recently proposed hybrid plasmonic based wave guiding mechanism, which combines the wave guiding properties of dielectric and plasmonic waveguides [13-15], is capable to resolve their respective issues of diffraction limit and large propagation loss. In these waveguides, the surface plasmonic (SP) mode supported by plasmonic waveguide (PW) combined with the dielectric mode supported by dielectric waveguide, and resulted mode is called a hybrid mode. It essentially provides a common platform to interconnect the electronics and photonics devices. To achieve ultra-small waveguide dimension, various hybrid plasmonic waveguides (HPWs) have been proposed in literature, such as hybrid metal-insulator-metal [14-17], hybrid dielectric loaded plasmonic structure [18-20], hybrid metal cap plasmonic waveguide [21], hybrid insulator-metal-insulator [22, 23], etc. Out of these possible structures of HPWs, the HIMIPW offers the least propagation loss with tight light confinement at true nano-scale regions. The optical devices based on hybrid plasmonic mechanism, such as all-optical logic gates [24-26], power splitter [27-30], ring resonator [31], etc. have been recently discussed in literature. The flow of light has been significantly controlled by the hybrid insulator metal insulator plasmonic waveguide structures. Therefore, this mechanism will be helpful to design a solar cells for energy harvesting by engineering the structures. The sensitivity of bio-sensor is higher than a conventional plasmonic sensor and it is capable of obtaining more information about biological molecules compared to conventional plasmonic sensors [32, 33]. The HPWs placed on silicon-on-insulator (SOI) are useful for achievement of dense monolithic integration of passive devices due to their ultra-small dimension and adaptability with CMOS technology.

In this current work, the optical properties of the fundamental hybrid mode profile in the HIMIPW have been studied, with the help of finite element method (FEM). The investigations have been done by varying the dimension of the

waveguide, to achieve the small propagation loss with high normalized intensity. The HIMIPW gives a large normalized intensity in the low-index/spacer region, due to the field enrichment caused by the surface plasmon polaritons and the discontinuity of the electric field in the spacer region. In order to comprehend the dense hybrid plasmonic integrated circuits, the coupling length between two identically parallel HIMIPWs have been estimated by varying an edge-to-edge separation distance. The smaller coupling length leads high crosstalk between two HPWs. Further, to improve the coupling length, a metallic strip has been inserted between the two parallel HIMIPWs and the impact of different metals, in the metallic strip, on the coupling length has been investigated.

2 Waveguide modeling, numerical method and fabrication process

The cross sectional view of HIMIPW, consists of insulator-metal-insulator (SiO_2 – Ag – SiO_2) layers, inserted between two dielectric regions of silicon (Si), as depicted in Fig. 1(a). Figure 1(b) indicates that normalized power is concentrated in low-index regions. The dielectric materials, Silica (SiO_2) and Silicon (Si) are used respectively as the low- and high- index materials, having their corresponding refractive indices of 1.44 and 3.48 [34]. However, the Drude model can be used to calculate the permittivity of metal (silver (Ag)), and can be expressed as [29],

$$\varepsilon = \varepsilon_\infty - \frac{{w_p}^2}{w^2 + jw\gamma} \tag{1}$$

where, ε_∞ , w_p and γ are dielectric constant at infinite angular frequency, bulk plasma frequency and damping frequency of silver respectively, with their respective values of 3.7, 1.3826×10^{16} Hz and 2.7438×10^{13} per sec. Hence, the permittivity of silver can be extracted as $-129 + 3.3i$ at 1.55 μm of wavelength. Silver (Ag) has been used as plasmonic material, as it offers the low propagation loss and high field enhancement for plasmonic based devices, whereas, air and silica are used for cladding and substrate materials, respectively. The thickness of low-index regions are assumed as t_{l1} and t_{l2}, and the same for the high-index regions are t_{h1} and t_{h2} . w is considered as the width of the HIMIPW. For the design and analysis of optical properties of HIMIPW, the electromagnetic wave frequency domain solver of COMSOL Multiphysics has been used with extra fine mesh size and the boundary condition of the perfect electric conductor has been applied.

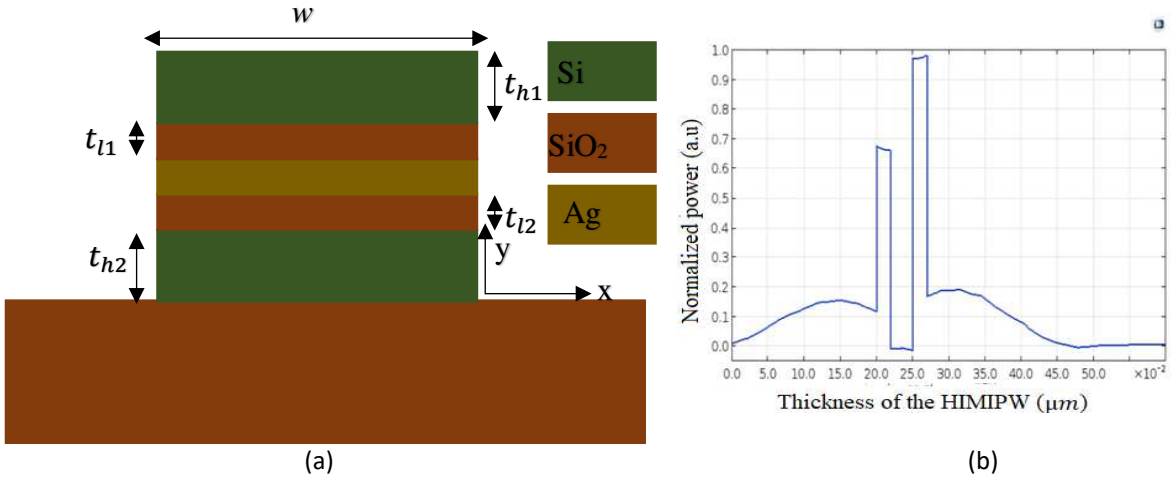

Fig. 1. (a) Cross sectional view (b) Normalized power at $t_{h1} = t_{h2} = 0.2\ \mu m$, and $t_{l1} = t_{l2} = 0.02\ \mu m$ of HIMIPW.

3 Optical properties of hybrid mode of the HIMIPW

The investigations on optical properties of the fundamental hybrid mode of the HIMIPW have been done by changing the waveguide width (w) and thickness of dielectric regions. The metal thickness is taken as 0.03 μm to guarantee no effect on the plasmonic mode. The skin depth in plasmonic metal (Ag) remains roughly uniform at 0.02 μm in the near-infrared regions [34]. The modal properties of the quasi-TM mode of the HIMIPW has been explored in terms of mode effective index, light confinement and normalized intensity in the spacer regions. The real part of mode

effective index can be presented as ($Re(N_{eff}) = Re(\beta)/k$), here, k and β are wave number of the free-space and propagation constant, respectively. Furthermore, the propagation length (L_p) of the waveguide is an important features to design and analyze HPWs and devices, which can be determined as a length (distance) at which the guided optical power is decreased to $\frac{1}{e}$ of the initial optical power and mathematically, denoted as below [14],

$$L_p = \frac{\lambda}{4\pi \times Im(N_{eff})} \tag{2}$$

where, $Im(N_{eff})$ represents the imaginary part of mode effective index and λ is the working wavelength. On the other side, the confinement factor (CF) of the HPW is another key aspect of the optimal design of HIMIPWs. It can be defined as the quotient of the total optical power inside the spacer regions to the input optical power of the HPW and expressed as [35],

$$CF(\%) = \frac{\iint |\langle P_{zi}(x,y)dxdy\rangle|}{\iint_{-\infty}^{\infty} |\langle P_z(x,y)dxdy\rangle|} \times 100 \tag{3}$$

where, $P_{zi}(x,y)$ and $P_z(x,y)$ are time-averaged Poynting's vector along the positive z-axis respectively in spacer region and whole waveguide geometry. Parallel to the CF, the normalized intensity (I) in the low-index region of the HIMIPW can be described as the ratio of normalized power (i.e., confinement factor) to the area of the low-index region [36].

3.1 Effect of waveguide width on fundamental hybrid mode profile

In this subsection, the impact of w on the fundamental hybrid mode profile has been examined by considering the thicknesses of dielectric regions as, $t_{h1} = t_{h2} = t_h = 0.2\ \mu m$, and $t_{l1} = t_{l2} = t_l = 0.02\ \mu m$, and the w has been varied from 0.1 µm to 0.9 µm at working wavelength 1.55 µm. With respect to the variations in w, the behavior of real-part of effective index and propagation length have been depicted in Fig. 2 (a), whereas, the same for the confinement factor and normalized intensity have been shown in Fig. 2 (b). From the Fig. 2 (a), it is clear that the propagation length (line in red colour) and the real part of effective index (dotted line in black colour) are initially decreasing and increasing, respectively with increases the value of w, and then saturates for w > 0.7 µm. Similarly, the percentage of light confinement (dotted line in black colour) in the spacer region initially increasing and then saturates with w > 0.7 µm, as depicted in Fig. 2(b). Moreover, the confinement factor of light wave is mainly dependent upon the power inside the spacer region, which is directly reliant on the effective index. Further, the variations in normalized intensity in terms of w have been depicted in Fig. 2(b). Figure 2 (b) indicates that the normalized intensity (line in red colour) in the low-index region, firstly increasing and goes to maximum value and then, decreasing with increases in the w. It is mainly due to the fact that for larger values of w, the CF is almost constant, but at the same time the area of spacer region increases with the increase in w. This leads to decrease in the value of normalized intensity and at w = 0.2 µm, the maximum value of the normalized intensity has been obtained as 67.5 μm^{-1}. Therefore, for the further investigations of the optical properties of HIMIPW, w is considered as 0.2 µm.

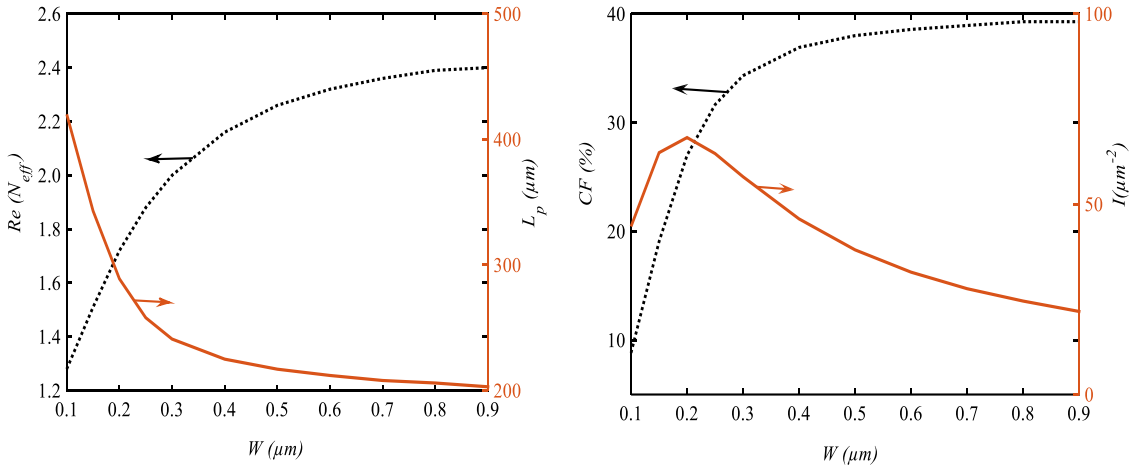

(a) (b)

Fig. 2 (a) Variations in real part of effective index and propagation length (b) Variations in confinement factor in percentage and normalized intensity vs. width of the HIMIPW.

3.2 Effect of dielectric thicknesses on fundamental hybrid mode profile

As discussed in the last subsection, w has been fixed as 0.2 µm, to investigate the impact of thicknesses of dielectric layers on optical properties of the fundamental mode. Figure 3 shows the variations in the real part of effective index and propagation length in terms of different thicknesses of low- and high-index regions of HIMIPW. From Fig. 3 (a), it is clear that $Re(N_{eff})$ decreases with the increase in the values of t_l, and it increases with the increase in t_h. If t_h is high and t_l is low, then HPW behaves as conventional plasmonic nature (due to Ag-Si). Further, if both t_h and t_l are high, then also, the HPW turns towards the conventional plasmonic waveguide (due to Ag-SiO_2). The relationship between the propagation length and the thicknesses of the low- and high-index layers have been depicted in Fig. 3 (b), where the increase in propagation length has been observed with the increasing t_h. This is mainly due to the dominating nature of dielectric waveguide (due to Si-SiO_2) on the HPW. However, if the t_l is increasing, then the nature of propagation length is dependent on the t_h. For example, if $t_{h1} = t_{h2} = t_h < 0.15\ \mu m$, propagation length is initially increasing, then saturates with increases of t_l values; however, for $t_h > 0.15\ \mu m$, propagation length is firstly increasing up to maximum value then decreasing with increases the value of t_l. This nature of propagation length is due to the change in nature of HPW towards the plasmonic and dielectric behaviors, with the varyingt_h and t_l, as if t_h > 0.2 µm, at low value of t_l, the nature of mode is like conventional plasmonic mode (due to Ag-Si) and with the increases in t_l, then conventional plasmonic mode turns towards hybrid plasmonic mode and further, t_l > 0.06 µm, the hybrid plasmonic mode turns toward plasmonic mode (due to Ag-SiO_2).

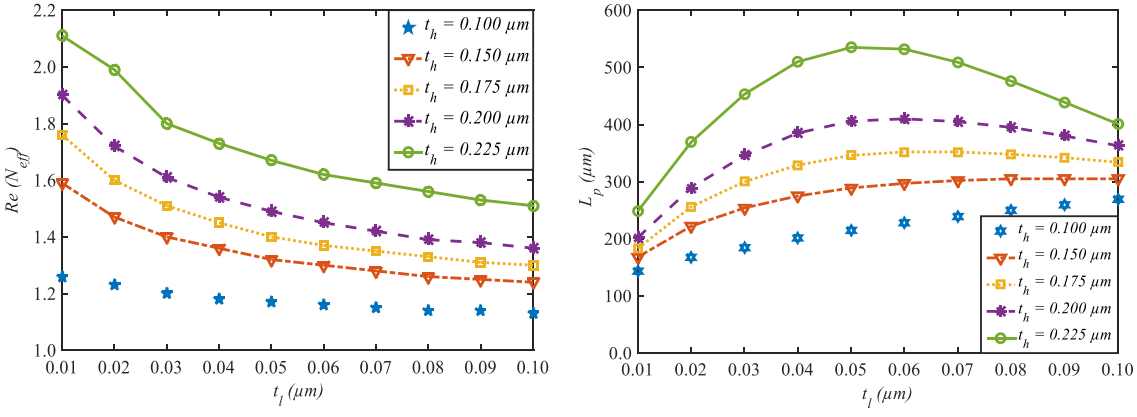

(a) (b)

Fig. 3. (a) Variations in real part of effective index (b) Variations in propagation length vs. thickness of dielectric regions of the HIMIPW.

Further, from Fig. 4 shows the relation of CF and normalized intensity with the thicknesses of dielectric layers. From the Fig. 4(a), it is clear that with the increase in t_h values, the confinement of light initially increasing, but after $t_h >$ 0.2 μ m, then CF is decreasing, as light starts to concentrate towards the high-index region. At $t_h = 0.1\ \mu m$, confinement factor is firstly increasing with t_l and after some values ($t_l > 0.06\ \mu m$), the behavior of confinement factor is linear with a small constant slope. The confinement factor at $t_h = 0.1\ \mu m$ is small as compared to other values. Further, with the increase in t_l values, light confinement factor first increases and after a certain value of t_l, it is decreasing with increases in value of t_l. Therefore, it can be concluded that the maximum confinement factor can be achieved at the waveguide dimension of t_h = 0.2 μm with t_l in between 0.02 to 0.04 μm. The variations in the normalized intensity can be visualized in Fig. 4 (b), which shows that with the increasing t_l values, the normalized intensity decreases. Moreover, in terms of thickness of the high index layer, the normalized intensity is quite lesser for $t_h <$ 0.1 μm and $t_h >$ 0.2 μm, which is mainly due to the lesser confinement of optical power in spacer region. The maximum value of normalized intensity has been obtained at t_h = 0.2 μm with the lower value of t_l.

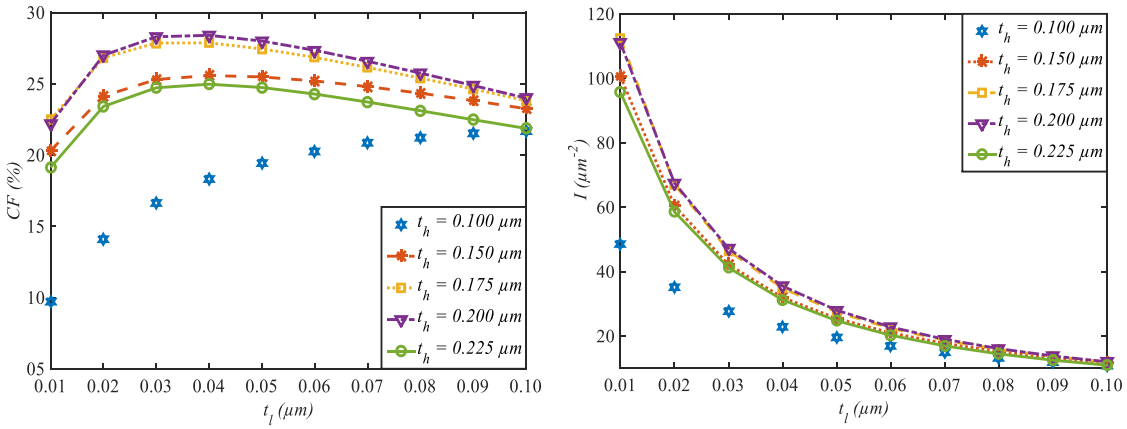

(a) (b)

Fig. 4. (a) Variations in confinement factor (b) Variations in normalized intensity vs. thickness of dielectric regions of the HIMIPW.

3.3 Effect of upper dielectric thicknesses on fundamental hybrid mode profile

In this section, the design of asymmetrical HIMIPW has been explored by keeping the width and the thicknesses of lower dielectric layers fixed as, w = 0.2 μm, $t_{h2} = 0.2\ \mu m$ and$t_{l2} = 0.02\ \mu m$. The designs of asymmetric HIMIPW have been investigated, first by varying t_{l1}, from 0.02 μm to 0.1μm, while keeping t_{h1} fixed as 0.2 μm , and illustrated in Fig. 5 (a). The figure indicates, the relation between propagation length and light confinement of the quasi-TM modes are inversely proportional. The propagation length is initially decreasing to a minimum value and again increasing with increases in value of t_{l1}. This is mainly due to the fact that for lower t_{l1} values, the hybrid plasmonic mode turns towards the conventional plasmonic mode (due to Ag-SiO_2). Moreover, after $t_{l1} > 0.06\ \mu m$, the propagation length increases, as the conventional plasmonic mode turns toward dielectric mode, which is basically caused by the lesser or negligible impact of metal in the presence of thicker spacer region. The variations in CF show just opposite nature as that of the propagation length. The second approach for design investigations is by considering $t_{l1} = 0.02\ \mu m$ and varying the values of t_{h1} from 0.1 to 0.3 μm, as depicted in Fig. 5 (b). From the figure, it can be observed that the propagation length increases to a maximum value (370 μm) at t_{h1} (= 0.225 μm), and then, it reduces gradually as the hybrid mode turns toward the conventional plasmonic mode (due to Ag-Si). However, the maximum CF in the spacer region has been observed as ~ 27.5 %, nearly at $t_{h1} = 0.175 - 0.2$ μm. Therefore, from the above analysis, it can be predicted that to achieve the miniaturized optical waveguide structure, the symmetrical HIMIPW is more beneficial than its asymmetrical counterpart. The optimized parameters for the symmetrical HIMIPW are W = 0.2 μm, $t_{h1} = t_{h2} = t_h = 0.2\ \mu m$ and $t_{l1} = t_{l2} = t_l = 0.02\ \mu m$ and the optimized values of propagation length, confinement factor (%) and normalized intensity are 289.26 μm, 28 % and 67.5 μm^{-2}, respectively. Comparison of

modal properties (propagation length and normalized intensity) of the fundamental mode of the present work with the recently reported works shown in Table 1.

The table clearly shows that the propagation length achieved in the current work is significantly better than that reported in recent literature. Also, in terms of the normalized intensity, the current work exhibits the considerably improved performance.

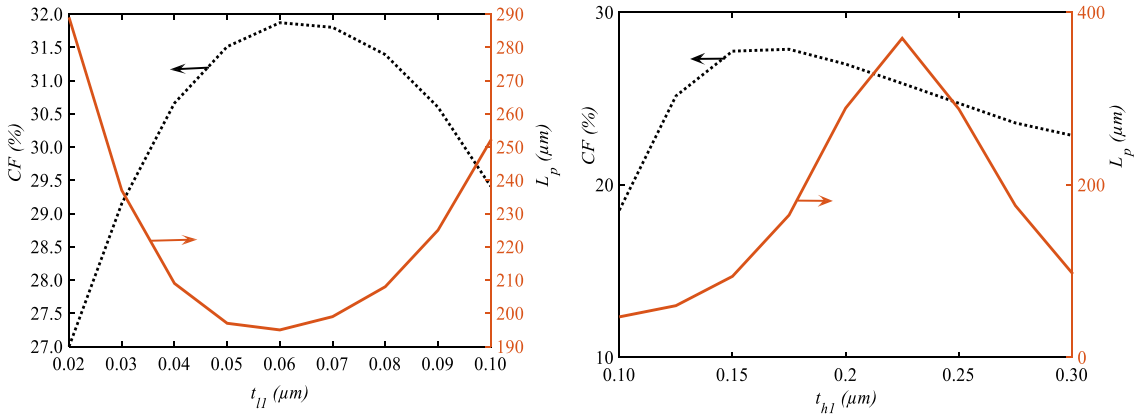

(a) (b)

Fig. 5. (a) Variations in confinement factor and propagation length vs. t_{l1} of the HIMIPW (b) Variations in confinement factor and propagation length vs. t_{h1} of the HIMIPW.

Table 1 Comparison of optical properties of the presented HIMIPW with different reported works.

Reported literature	Propagation length (μm)	Normalized intensity (μm^{-2})
[8]	5	-
[15]	185.56	132.5
[16]	40	74
[20]	64	36
[25]	11	-
[26]	23	-
[28]	20	-
[36]	-	20
[39]	46.7	-
Present work	289.26	67.5

To analyze the behavior of the localized surface plasmon resonance at the surface of the silver-Silica interfaces by varying of wavelength at optimum waveguide dimension $W = 0.2$ μm, $t_h = 0.2$ μm and $t_l = 0.02$ μm. The electric field intensity is firstly increasing up-to maximum value, then decreasing with increases the working wavelength, which is shown in Fig. (6). It provides highly localized electric field intensity around 1550 nm. Hence, the performance of the HIMIPW structure, at the working wavelength (1550 nm), is more efficient.

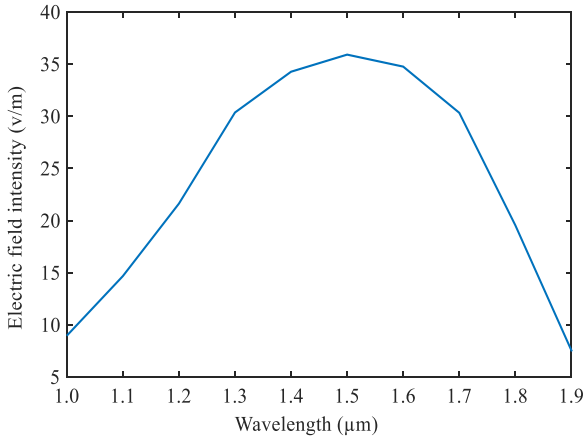

Fig. 6. Variations in electric field intensity vs. wavelength at $w = 0.2$ μm, $t_l = 0.02$ μm, and $t_h = 0.02$ μm.

4. Crosstalk between adjacent identical parallel HIMIPWs

In order to search the possibilities to realize the highly dense monolithic integration of the presented HIMIPWs, the crosstalk performance between two identical parallel HIMIPWs have been done, for a separation distance(d). Figure 7 shows the cross-sectional view of coupling arrangement between two parallel HIMIPWs. To analyze the crosstalk between two HPWs, the coupling length has to be determined, as provided in Eq. (4) [14, 16]. For the minimum/negligible crosstalk between the two HPWs, the coupling length must be significantly larger [37]. The coupling length (L_c) is defined as the distance (length) at which the maximum optical power is transported from one HIMIPW to another and it can be expressed as [19],

$$L_c = \frac{\pi}{|\beta_s - \beta_a|} \tag{4}$$

where, β_s and β_a are the propagation constants of symmetric and antisymmetric quasi-TM modes respectively. To examine the modal properties of the symmetric and antisymmetric modes, the separation distance (d) has been varied from 0.1 μm to 0.6 μm. Figure 8 clearly indicates the mode profile for the symmetric and antisymmetric quasi-TM mode. Further, Table 2 presents the values of coupling lengths and effective index of symmetric and antisymmetric modes for a wide range of d. From the table, it has been observed that if d increases, the real part of effective index of symmetric mode decreases and that of the antisymmetric mode increases. With further increase in 'd' values, at d = 0.80 μm, the effective index of both modes achieves the value of 2.41, which is known as the index of decoupled hybrid plasmonic mode. From the imaginary part of effective index, it can be established that the propagation loss of antisymmetric mode is larger than that of the symmetric mode. On the other hand, with the increases in 'd', the propagation loss of symmetric mode increases and that of antisymmetric mode decreases and both converges at d = 0.8 μm (not mention in table). The relationship between the coupling length and separation distance has been plotted in Fig. 9, which shows the exponentially increasing nature of the coupling length with separation distance (d). This is mainly due to the high propagation loss in both symmetric and antisymmetric modes. The 3-D view of symmetric modes, and antisymmetric modes at d = 0.1, 0.5, 0.8 μm, have been depicted respectively in Figs. 10 (a)-(c) and Figs. 10 (d)-(f). From the Fig. 10 (c) and (f), it is clear that at d = 0.8 μm, the maximum power from one HIMIPW has been transferred to another.

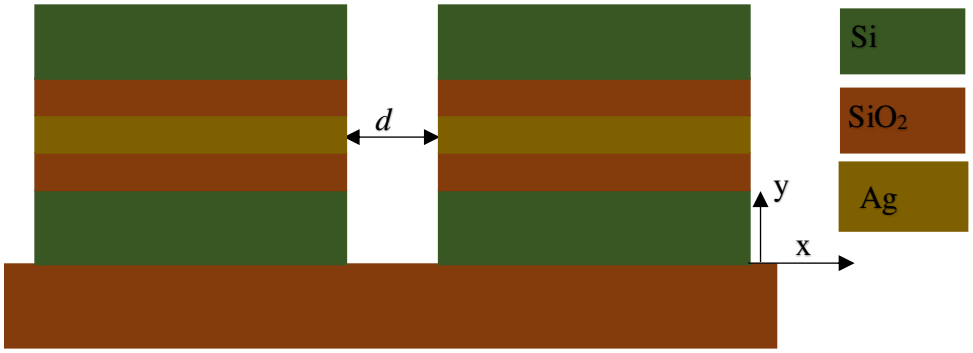

Fig. 7. Cross-sectional view of two identical parallel HIMIPWs with separation distance of d.

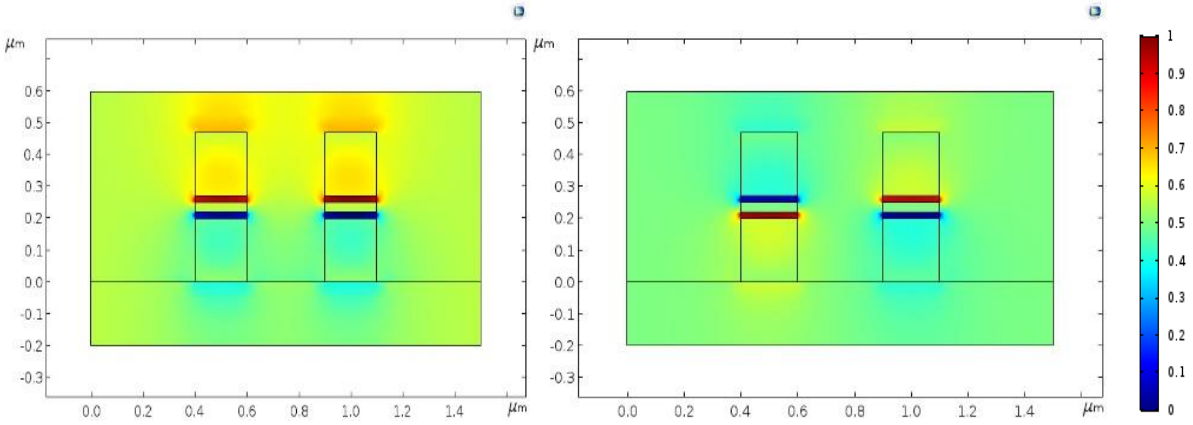

Fig. 8. (a) Quasi-TM mode profile of symmetric mode (b) Quasi-TM mode profile of antisymmetric mode at d = 0.3 μm.

Table 2 Effective index of symmetric and antisymmetric modes of the HIMIPW.

d (μm)	n_{symm}	n_{asymm}	L_c (μm)
0.10	2.4433-0.010306i	2.3958-0.011703i	16.32
0.15	2.4265-0.010612i	2.4020-0.011430i	31.63
0.20	2.4188-0.010792i	2.4063-0.011278i	62.00
0.25	2.4152-0.010896i	2.4088-0.011188i	121.09
0.30	2.4135-0.010959i	2.4100-0.011136i	221.43
0.35	2.4126-0.010943i	2.4107-0.011103i	407.89
0.40	2.4122-0.011016i	2.4111-0.011085i	704.55
0.45	2.4119-0.011030i	2.4112-0.011074i	1107.14
0.50	2.4118-0.011041i	2.4114-0.011069i	1937.50
0.55	2.4117-0.011048i	2.4114-0.011048i	2583.33
0.60	2.4116-0.011058i	2.4114-0.011068i	3875.00

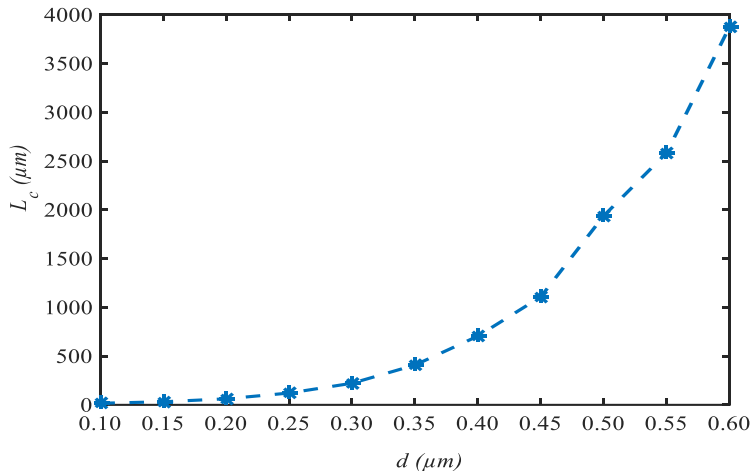

Fig. 9. Varaiations in Coupling length vs. separation distance between two parrel HIMIPWs.

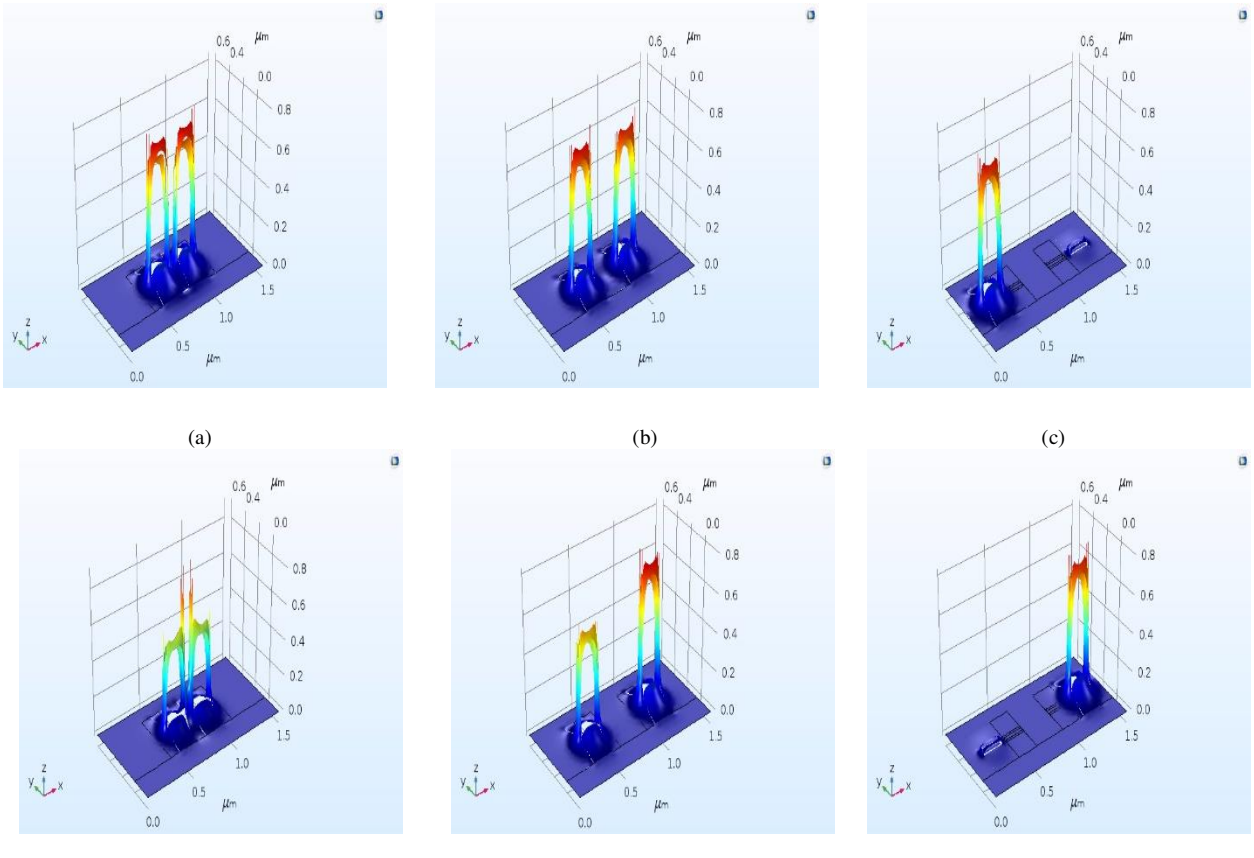

Fig. 10. Normalized power of the quasi-TM mode (a) – (c) symmetric mode at d = 0.1, 0.5, 0.8 µm, respectively, and (d)-(f) antisymmetric mode at d = 0.1,0.5,0.8 µm, respectively.

Further, to reduce the crosstalk and hence, to increase coupling length between two HIMIPWs, a metallic strip between the two HPWs has been inserted [35], as depicted in Fig. 11. Due to presence of middle metallic strip, the increase in coupling length can be anticipated. This is mainly based on the fact that in the dielectric region the field attenuation is much slower than that in the metal region. To analyze the impact of metallic strip on the coupling length, the separation distance (d) has been fixed at 0.30 µm , whereas the width (W_m) and height (h) of metallic strip have been varied respectively from 0.04 µm to 0.20 µm and 0.10 µm to 0.60 µm, for different considered metals for metallic

strip, such as Aluminium (Al), Copper (Cu), Gold (Au) and Silver (Ag). The refractive indices of Al, Cu and Au have been considered respectively as 1.5785+15.658i, 0.7158+10.655i and 0.5241+10.745i, at 1.55 µm of wavelength [38]. Figure 12 clearly indicates that the electromagnetic waves propagate through one waveguide to other in the presence of metallic strip. Mode profile for the symmetric and antisymmetric quasi-TM mode with inserted metallic strip between two waveguides have shown in Figs. 12 (a) and (b), respectively. Figure 13 illustrates that the variations in the coupling length of the HIMIPWs, which is increasing with the increase in the width and height of the inserted metallic strip. Further, Tables 3 and 4 indicate that after inserting the metallic strip, the values of coupling lengths have been improved for all the considered metals, as compared to that without the metallic strip (L_c = 221.43 µm), for the same separation distance (d = 0.3 µm). Table 3 indicates that the coupling length with Al as metallic strip, is greater than that with other metals. This is mainly due to the fact that Al has higher values of imaginary part of the refractive index for both the symmetric and antisymmetric modes, which further causes to the higher propagation loss. From the Table 4, it has been observed that coupling length increases with the increase in height of inserted metal; however, for h = 0.27 to 0.37 µm, coupling length has both decreasing and increasing nature for all the considered metals. This is mainly due to the fact that with this range of metallic strip height, the impact of the upper part of HIMIPW is quite lesser. However, d with further increase in 'h', the coupling length increases. Moreover, the presence of the metallic strip between two identical parallel HPWs, causes the inconvenience for the fabrication of such optical devices.

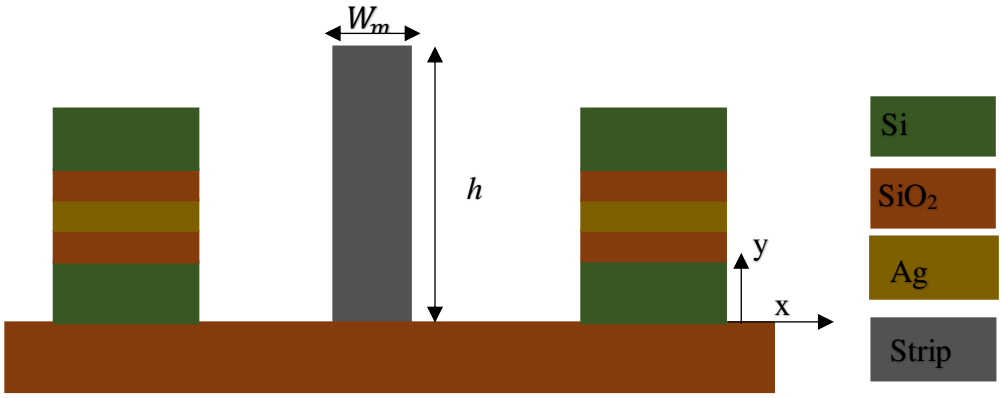

Fig. 11. Cross-sectional view of two identical parallel HIMIPWs with inserted metallic strip.

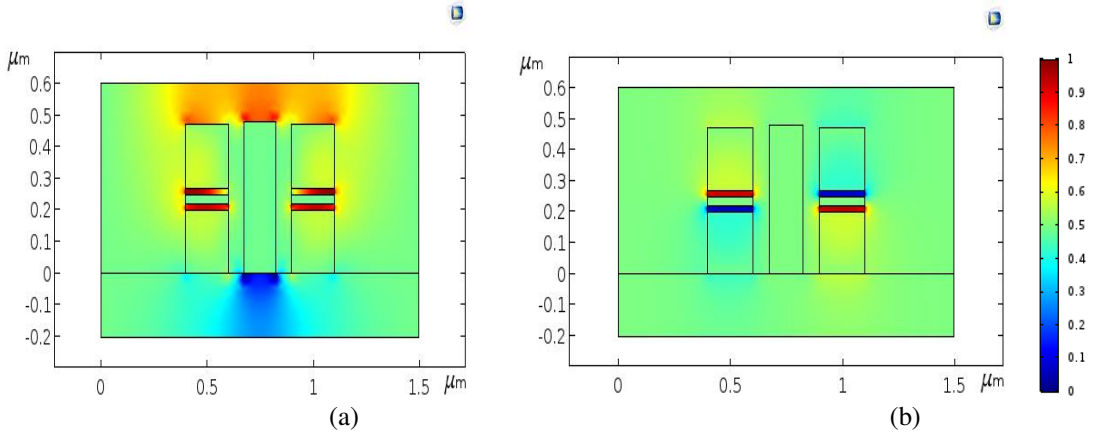

Fig. 12. Quasi-TM mode profiles of (a) symmetric mode (b) antisymmetric mode at d = 0.3 µm with inserted Al metallic strip

Table 3 Variations in coupling length with different metals for the inserted metallic strip by varying the width of metallic strip.

W_m(μm)	L_{Ag} (μm)	L_{Al} (μm)	L_{Cu} (μm)	L_{Au} (μm)	L_c (μm) without metallic strip
0.05	267.24	336.96	258.00	258.00	221.42
0.10	407.90	430.56	387.50	387.50	221.43
0.15	516.67	553.57	516.67	516.67	221.43

Table 4 Coupling length with different metals for the inserted metallic strip by varying height of metallic strip.

h (μm)	L_{Ag} (μm)	L_{Al} (μm)	L_{Cu} (μm)	L_{Au} (μm)	L_c (μm) without metallic strip
0.20	287.04	310.00	267.24	267.24	221.42
0.22	298.08	322.92	298.08	287.04	221.43
0.25	298.08	298.08	298.08	310.00	221.43
0.27	287.04	267.24	298.08	298.08	221.42
0.30	267.24	250.00	276.78	276.79	221.43
0.35	276.79	276.78	287.04	276.79	221.43
0.37	298.08	298.08	310.00	298.08	221.42
0.40	352.27	352.27	352.27	352.27	221.43
0.47	516.67	553.57	516.67	516.67	221.43
0.50	553.57	645.83	596.15	596.15	221.42
0.60	775.00	861.11	704.56	775.00	221.43

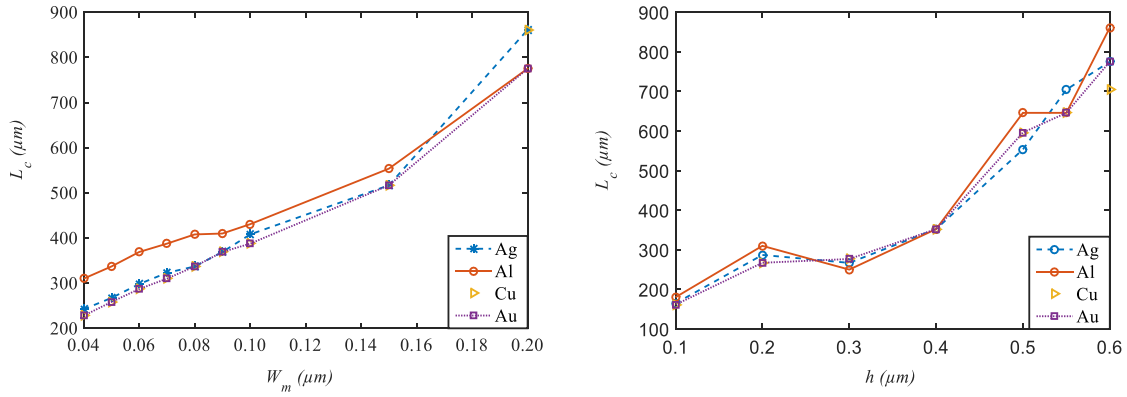

(a) (b)

Fig. 13. Variations in coupling length vs. (a) Width (b) Height of inserted metallic strip at the centre between two HIMIPW.

5 Conclusion

In the present work, the analysis of fundamental hybrid mode properties in HIMIPW has been done to obtain the significant light confinement of optical power in nano-scale low-index region (~ 20 nm) and high propagation length (~ 289 μm). The normalized intensity of roughly 67.50 μm^{-2}, at the working wavelength of 1.55 μm has been obtained, it is due to the field enrichment in the spacer regions of HIMIPW. However, the normalized intensity can be further improved by reducing the thickness of spacer region, up to ~ 10 nm, this is beneficial for many applications such as nonlinear optics, optical bio-sensing, etc. The electric field intensity has been achieved highest values at the working wavelength 1.55 μm and it indicates that the performance of the design waveguide is more efficient at target wavelength. The investigations, to achieve the suitable coupling length between two identical parallel HIMIPWs, has been done with different separation distances, which is further improved by inserting a metallic strip between the two parallel hybrid plasmonic waveguides at the same separation distance. Higher coupling length leads to low crosstalk between two hybrid plasmonic waveguide and it is useful to achieve

the larger integration on photonic chip. The maximum values of the coupling length have been attained, when the use of wider and thicker metallic strip in the center between two waveguides. The SOI-based HPWs are an advantageous for the realization of monolithic integration of passive devices and adaptable with CMOS technology.

Acknowledgments

The authors gratefully acknowledge, National Institute of Technology Patna, and Science and Engineering Research Board, Department of Science and Technology, Government of India for providing COMSOL Multiphysics simulation software, used in the current simulation work.

Author Contributions All authors are equally contributed in the manuscript.

Data Availability I reused existing data.

Conflict of Interest The authors declare that they have no conflicts of interest.

Consent for Publication Not Applicable.

Consent to Participate Not Applicable.

Compliance with Ethical Standards This article does not contain any studies involving animals or human participants performed by any of the authors.

Funding Statement No Funding was received

References

[1] Q. Li, M. Qiu, Structurally-tolerant vertical directional coupling between metal-insulator-metal Plasmonic waveguide and silicon dielectric waveguide, Optics Express 18 (2010) 15531-15543.

[2] N. Eti, H. Kuri, Model analysis of ridge and rib types of Silicon waveguides with void Compositions, IEEE Journal of Quantum Electronics 52 (2016) 8400207.

[3] K. Y. Jung, F. L. Teixeira, and R. M. Reano, Au/SiO_2 nanoring plasmon waveguides at optical communication band, Journal of Lightwave Technology, 25 (2007) 2757-2765.

[4] A. Ahmadivand, and S. Golmohammadi, Comprehensive investigation of nobel metal nanoparticles shape, size and material on the optical response of optical Y-splitter waveguides, Optics Communications, 310 (2014) 1-11.

[5] T- and Y-splitters based on an Au/SiO_2 nanoring chain at an optical communication band, Applied Optics, 51 (2012) 2784-2793.

[6] A. Ahmadivand, Hybrid photonic-plasmonic polarization beam splitter (HPPPBS) based on metal-silica-silicon interactions, Optics & Laser Technology, 58 (2014) 145-150.

[7] A. Ahmadivand, and S. Golmohammadi, Electromagnetic plasmon propagation and coupling through gold nanoring heptamers: a route to design optimized telecommunication photonic nanostructures, Applied Optics, 53 (2014) 3832-3840.

[8] A. V. Krasavin, A. V. Zayats, Silicon-based Plasmonic waveguides, Optics Express. 18 (2010) 11791-11799.

[9] S. Foroutana, G. Rostamib, M. Dolatyarib, A. Rostamia, All-Optical switching in metal nanoparticles plasmonic waveguide using EIT phenomenon, Optik 132 (2017) 291–298.

[10] T. Nurmohammadia, K. Abbasianb, Reza Yadipoura, A proposal for a demultiplexer based on plasmonic metal–insulator–metal waveguide-coupled ring resonator operating in near-infrared spectrum, Optik 142 (2017) 550–556.

[11] Y. Zeng, L. Wang, X. Xia, Z. Wang, Research transmission characteristics of a plasmonic multiple-ring shaped metal-insulator-metal waveguide, Optik 127 (2016) 1084–1086.

[12] J. Grandidier, S. Massenot, G. C. D. Francs, A. Bouhelier, J. C. Weeber, L. Markey, and A. Dereux, Dielectric-loaded surface plasmon polariton waveguides: Figures of merit and mode characterization by image and fourier plane leakage microscopy, Physical Review, 78 (2008) 245419.

[13] M. Z. Alam, J. A. Stewart, and M. Mojahedi, Theoretical analysis of hybrid Plasmonic waveguide, IEEE Journal of Selected Topics in Quantum Electronics, 19 (2013) 4602008.

[14] Y. Bian, Q. Gong, Optical performance of one-dimensional hybrid metal-insulator-metal structures at telecom wavelength, Optics Communications. 308 (2013) 30-35.

[15] P. sharma, V. D. Kumar, Investigation of multilayer planer hybrid Plasmonic waveguide and bends, IET Electronics Letters. 52 (2016) 732-734.

[16] P. Kumar, D. K. Singh, R. Ranjan, Optical performance of hybrid metal-insulator-metal plasmonic waveguide for low-loss and efficient photonic integration, Microw Opt Technol Lett. 62 (2020)1–9.

[17] P. Kumar, D. K. Singh and R. Ranjan, Mode Analysis of Hybrid Metal-Insulator-Metal Multilayer Plasmonic Waveguide, 2018 Conference on Information and Communication Technology (CICT), Jabalpur, India, 2018, pp. 1-4.

[18] T. Holmgaard, I. Bozhevolnyi, Theoretical analysis of dielectric-loaded surface plasmon-polariton waveguides, Physical Review. 75 (2007) 245405-1- 245405-12.

[19] P. Kumar, D. K. Singh, R. Ranjan, Optical performance of hybrid dielectric loaded plas-monic waveguide using PTFE for nano-scale light con-finement, Optoelectronics letters. 16 (2020)1–9.

[20] H. S. Chu, E. P. Li, P. Bai, R. Hegde, Optical performance of single-mode hybrid dielectric-loaded Plasmonic waveguide-based components, Applied Physics Letters. 96 (2010) 221103.

[21] D. Dai, S. He, A silicon-based hybrid Plasmonic waveguide with a metal cap for a nano-scale light confinement, Optics Express. 19 (2009) 16646-16653.

[22] M. Z. Alam, J.A. Stewart, M. Mojahedi, A marriage of convenience: hybridization of surface Plasmon and dielectric waveguide modes, Laser Photonics Reviews. 8 (2014) 394–408.

[23] M. T. Noghani, H. Mohammad, V. Samiei, Analysis and optimum design of hybrid Plasmonic slab waveguides, Plasmonics. 8 (2013) 1155–1168.

[24] P. Sharma, V. D. Kumar, All optical logic gates using hybrid metal insulator metal plasmonic waveguide, IEEE Photonics Technology Letters. 30 (2018) 959-962.

[25] Y. Fu, X. Hu, C. Lu, S. Yue, H. Yang, Q. Gong, All-optical logic gates based on nanoscale plasmonic slot waveguides, Nano Letters, 12 (2012) 5784–5790.

[26] C. Lu, X. Hu, S. Yue, Y. Fu, H. Yang, Q. Gong, Ferroelectric hybrid plasmonic waveguide for all-optical logic gate applications, Plasmonics, 8 (2013) 749–754.

[27] M. Singh, Design of hybrid multilayer plasmonic switch-cum-splitter with 90° bends,Optik - International Journal for Light and Electron Optics 178 (2019) 902–908.

[28] M. Nikoufard, M. Alamoun, S. Pourgholi, Multimode interference power-splitter using InP-based deeply etched hybrid plasmonic waveguide, IEEE Transaction on Nanotechnology. 16 (2017) 477-483.

[29] J. Tian, R. Yang, L. Song, W. Xue, Optical properties of a Y-splitter based on hybrid multilayer plasmonic waveguide, IEEE Journal of Quantum Electronics. 50 (2014) 898-903.

[30] J. Wang, X. Guan, Y. He, Y. Shi, Z. Wang, S. He, P. Holmstrom, L. Wosinski, L. Thylen, and D. Dai, Sub-μm^2 power splitters by usingsilicon hybrid Plasmonic waveguides, Optics Express, 19 (2011)838-847.

[31] Y. Guo, L. Yan, W. Pan, B. Luo, K. Wen, Z. Guo, X. Luo, Transmission characteristics of the aperture-coupled rectangular resonators based on metal-insulstor-metal waveguides, Optics Communications. 300 (2013) 277-281.

[32] S. Shukla, and P. Arora, Design and analysis of Aluminum-Silicon-Graphene based plasmonic device for biosensing applications in the optical communication band. Silicon. (2021). https://doi.org/10.1007/s12633-021-00953-4

[33] M. Esfandiyari, M. Norouzi, P. Haghdoust, and S. Jarchi, Study of a Surface plasmon resonance optical fiber sensor based on periodically grating and graphene. Silicon. 10 (2018) 2711-2716.

[34] H. S. Chu, E. P. Li, P. Bai, R. Hegde, Characterization of Planar Hybrid Dielectric-loaded Plasmonic nanoWaveguides used for nano-Photonic Circuits,IEEE MTT-S international microwave Symposium, Baltimore 1 (2011), (USA).

[35] X. Sun, M. Z. Alam, M. Mojahedi, J. S. Aitchison, Confinement and integration density of plasmonic waveguides, IEEE Journal of Selected Topics in Quantum Electronics. 21 (2015) 4600308.

[36] V. R. Ameida, Q. Xu, C. A. Barrios, M. Lipson, Guiding and confining light in void nanostructure, Optics Letters. 29 (2004) 1209-1211.

[37] Y. Song, M. Yan, Q. Yang, L. Tong, M. Qiu, Reducing crosstalk between nanowire-based hybrid plasmonic waveguides,Optics Communications 284 (2011) 480–484.

[38] M. N. Polyanskiy, Refractive index database, https://refractiveindex.info. Accessed on 2020-01-19

[39] J. Xiao, Q. Wei, D. Yang, P. Zhang, N. He, G. Zhang, T. Ren, X. Chen, A CMOS-compatible hybrid plasmonic slot waveguide with enhanced field confinement, IEEE Electronics Device Letters. 37 (2016) 456-458.

Figures

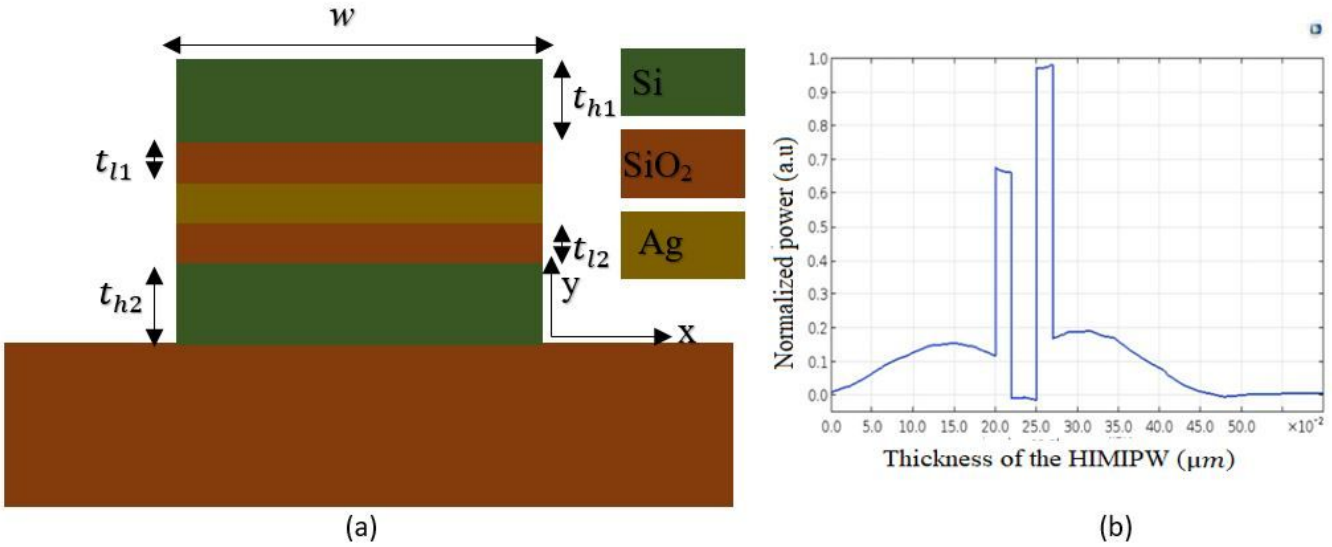

Figure 1

(a) Cross sectional view (b) Normalized power at t_h1= t_h2=0.2 μm, and t_l1= t_l2=0.02 μm of HIMIPW.

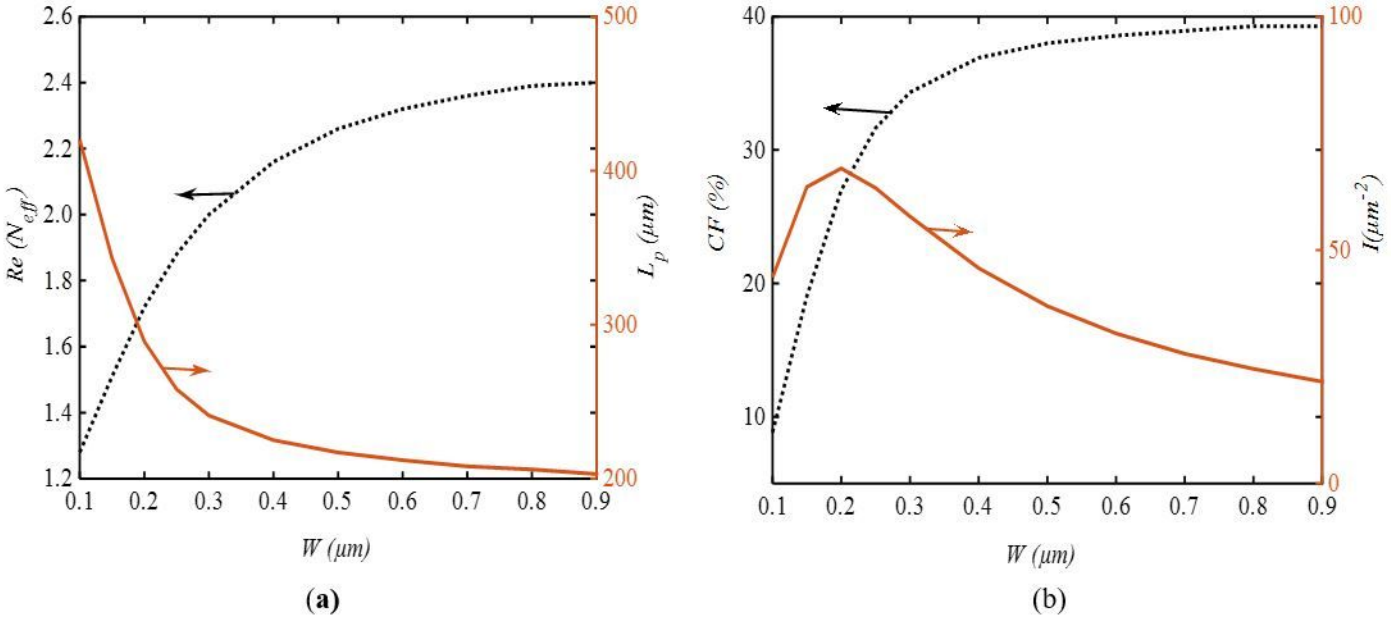

Figure 2

(a) Variations in real part of effective index and propagation length (b) Variations in confinement factor in percentage and normalized intensity vs. width of the HIMIPW.

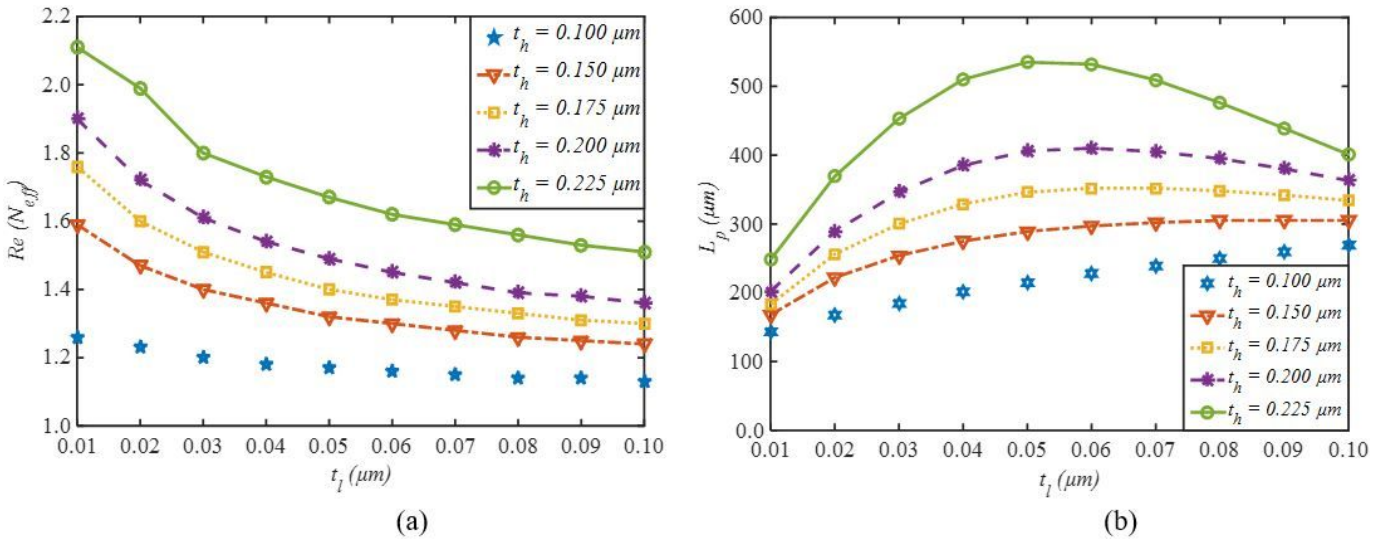

Figure 3

(a) Variations in real part of effective index (b) Variations in propagation length vs. thickness of dielectric regions of the HIMIPW.

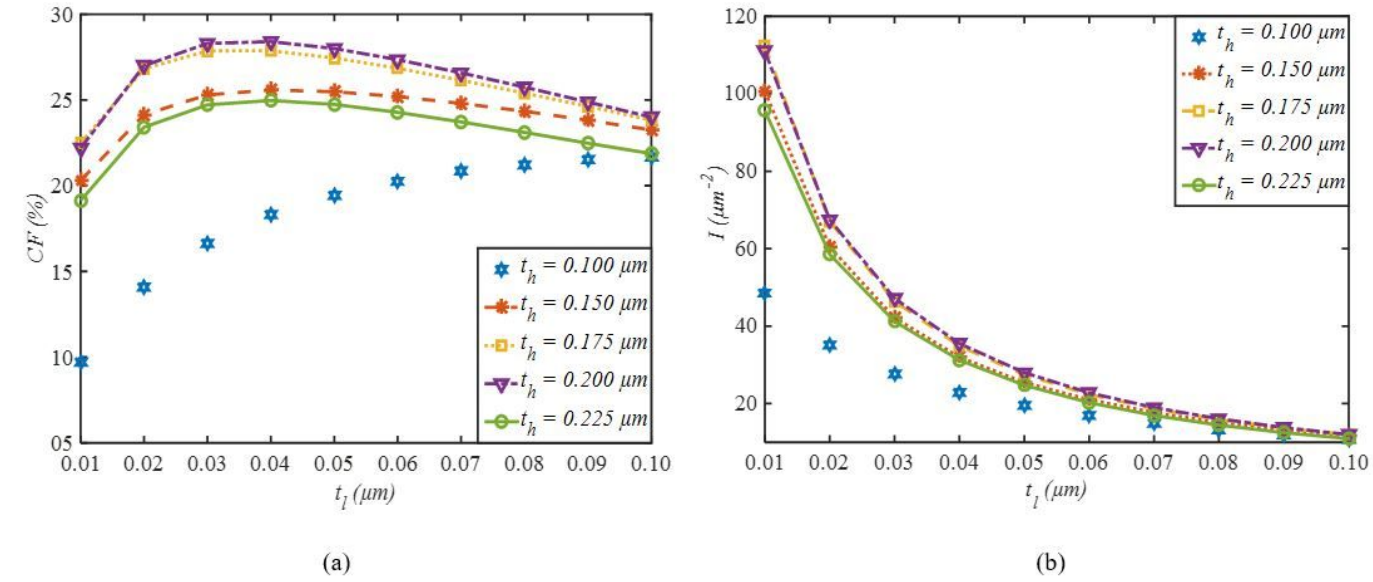

Figure 4

(a) Variations in confinement factor (b) Variations in normalized intensity vs. thickness of dielectric regions of the HIMIPW.

Figure 5

(a) Variations in confinement factor and propagation length vs. t_l1 of the HIMIPW (b) Variations in confinement factor and propagation length vs. t_h1 of the HIMIPW.

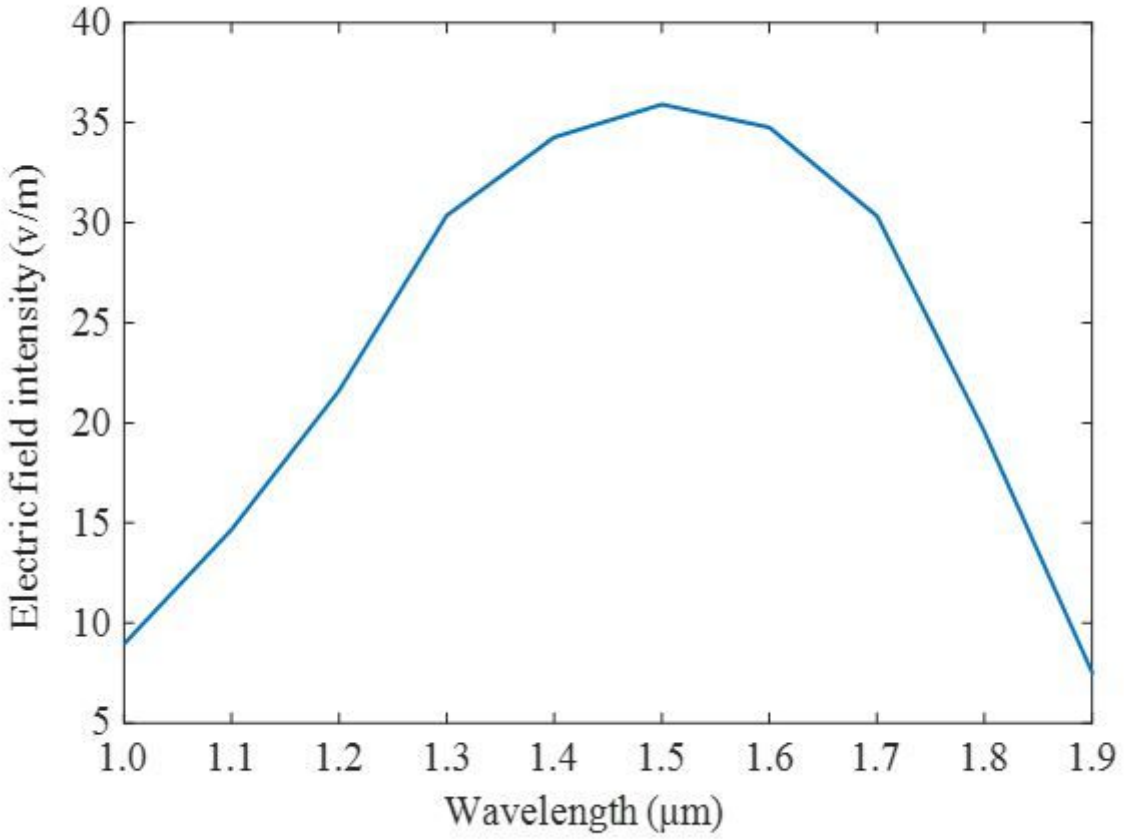

Figure 6

please see the manuscript file for the full caption

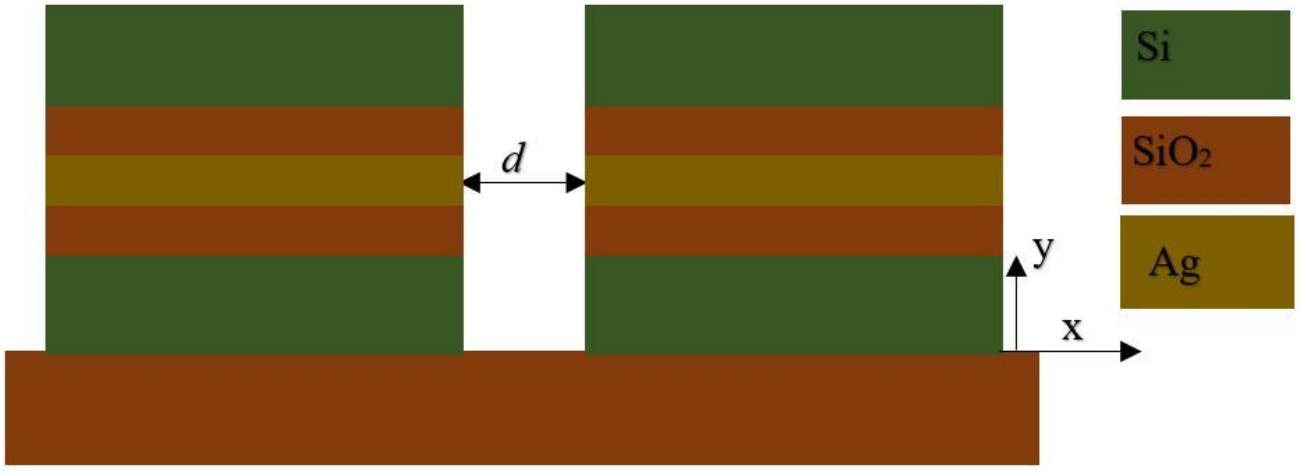

Figure 7

Cross-sectional view of two identical parallel HIMIPWs with separation distance of d.

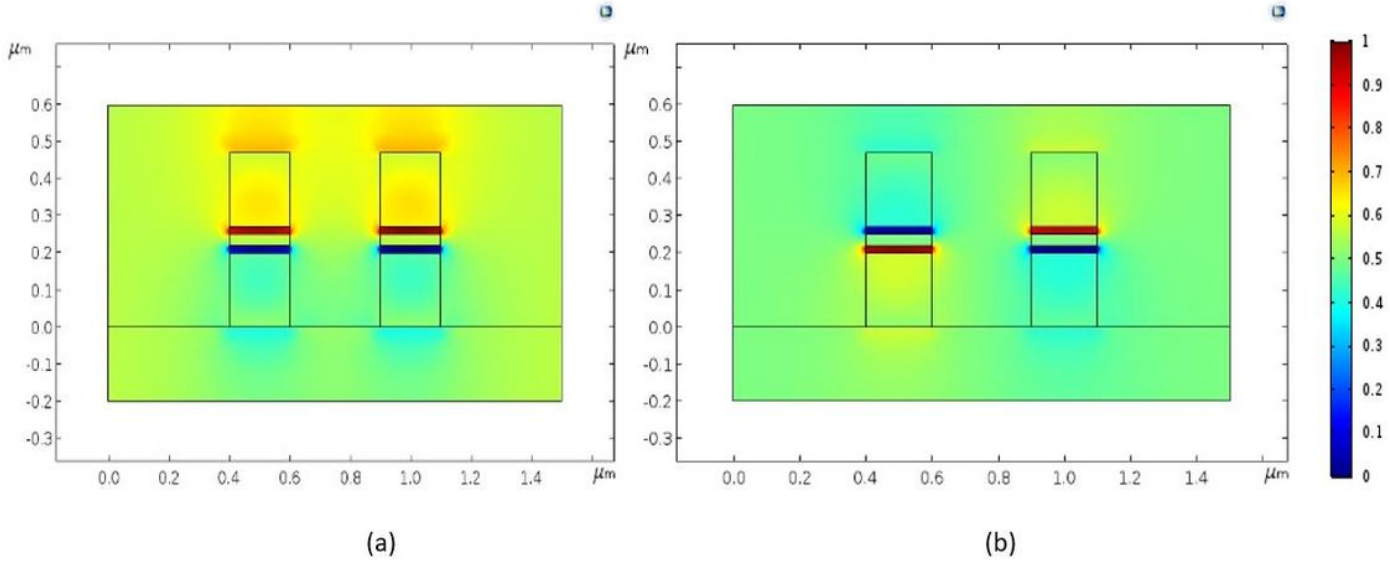

Figure 8

(a) Quasi-TM mode profile of symmetric mode (b) Quasi-TM mode profile of antisymmetric mode at d = 0.3 μm.

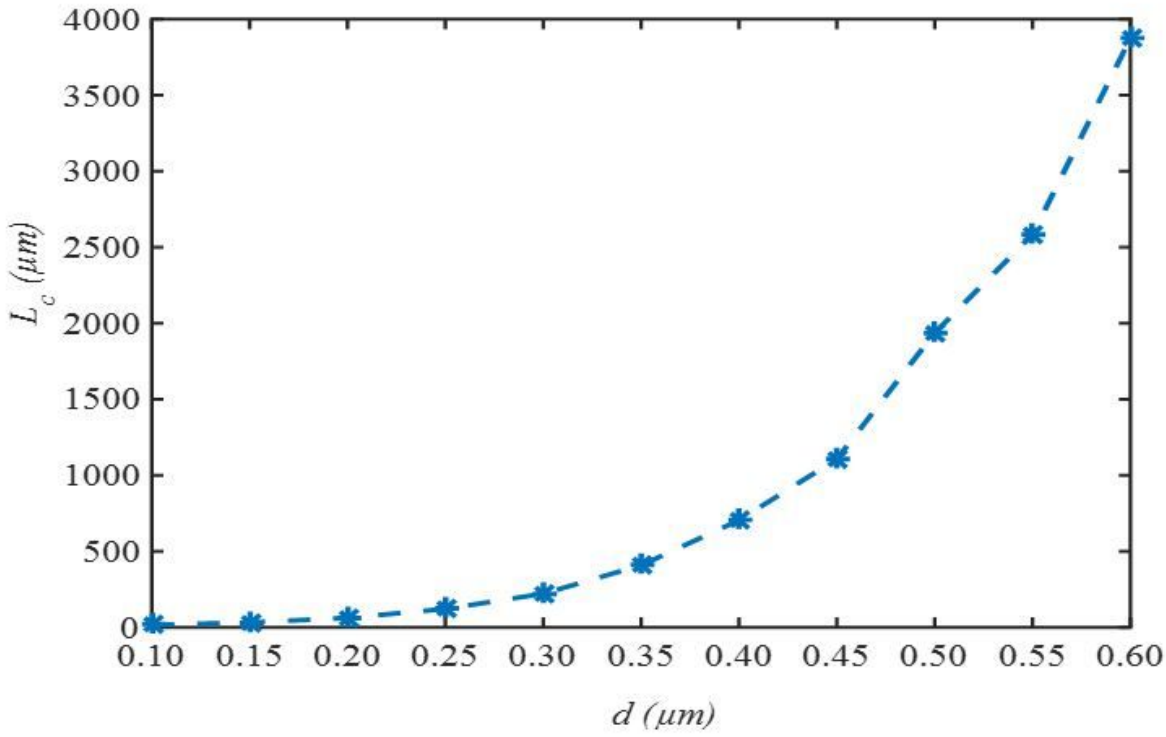

Figure 9

Varaiations in Coupling length vs. separation distance between two parrel HIMIPWs.

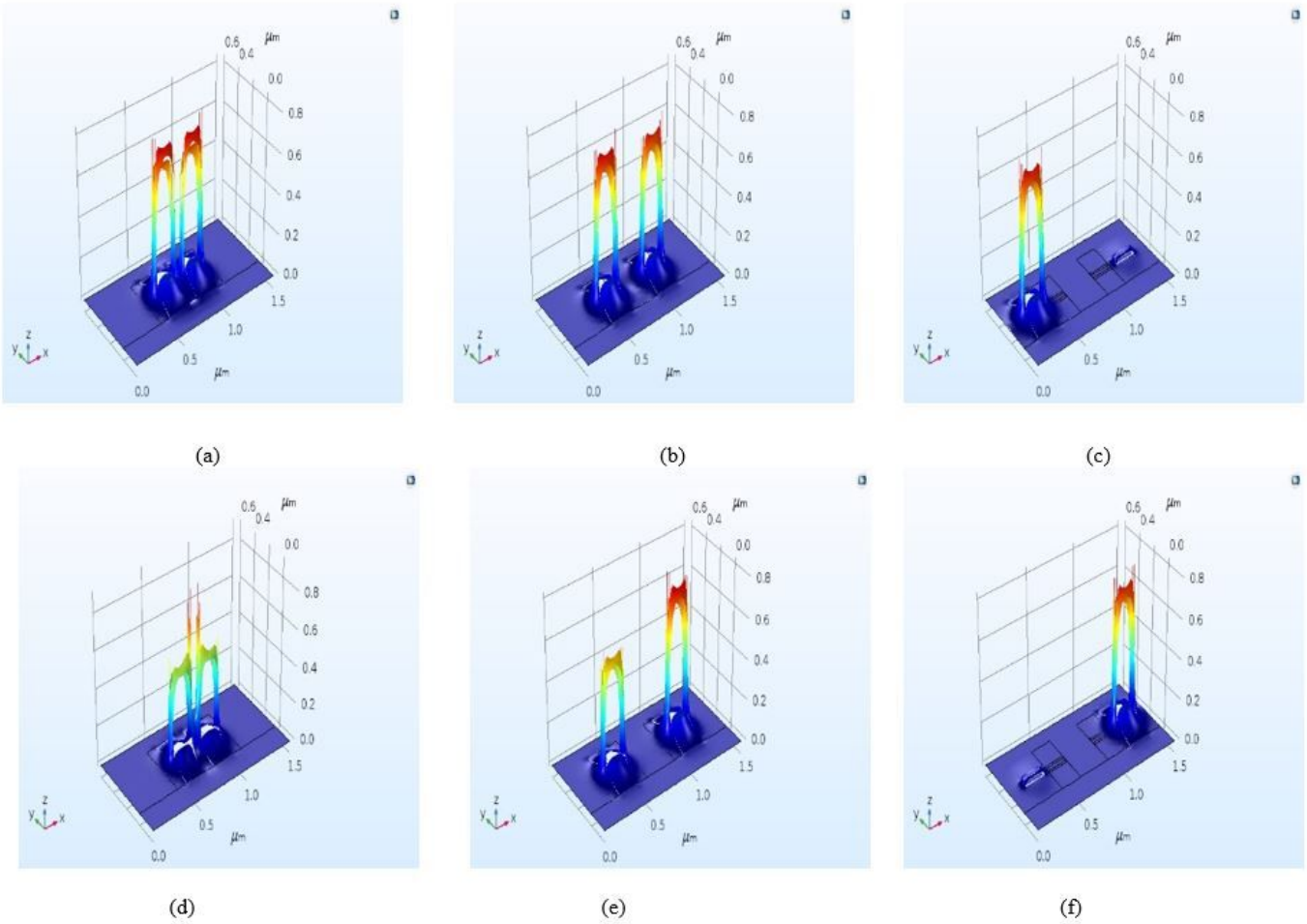

Figure 10

Normalized power of the quasi-TM mode (a) – (c) symmetric mode at d = 0.1, 0.5, 0.8 μm, respectively, and (d)-(f) antisymmetric mode at d = 0.1,0.5,0.8 μm, respectively.

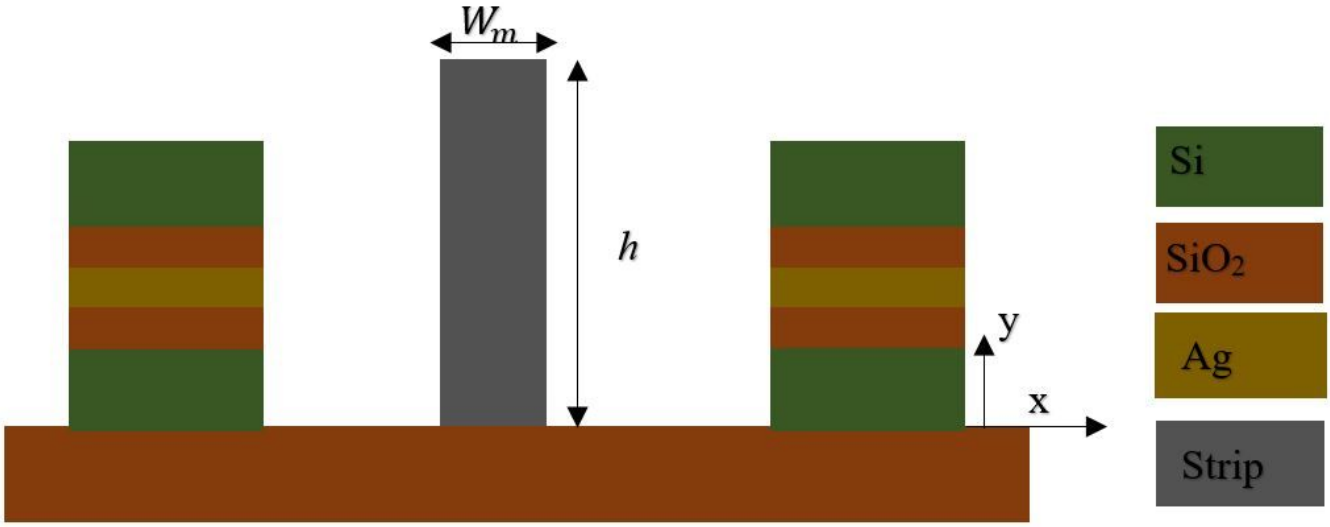

Figure 11

Cross-sectional view of two identical parallel HIMIPWs with inserted metallic strip.

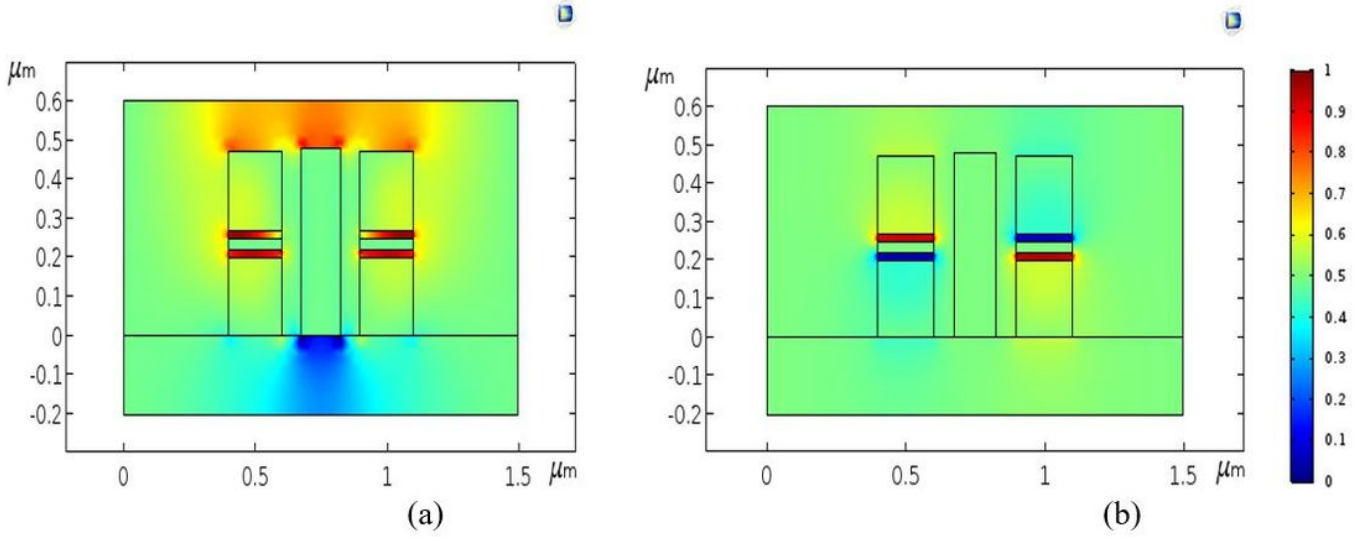

Figure 12

Quasi-TM mode profiles of (a) symmetric mode (b) antisymmetric mode at d = 0.3 μm with inserted Al metallic strip

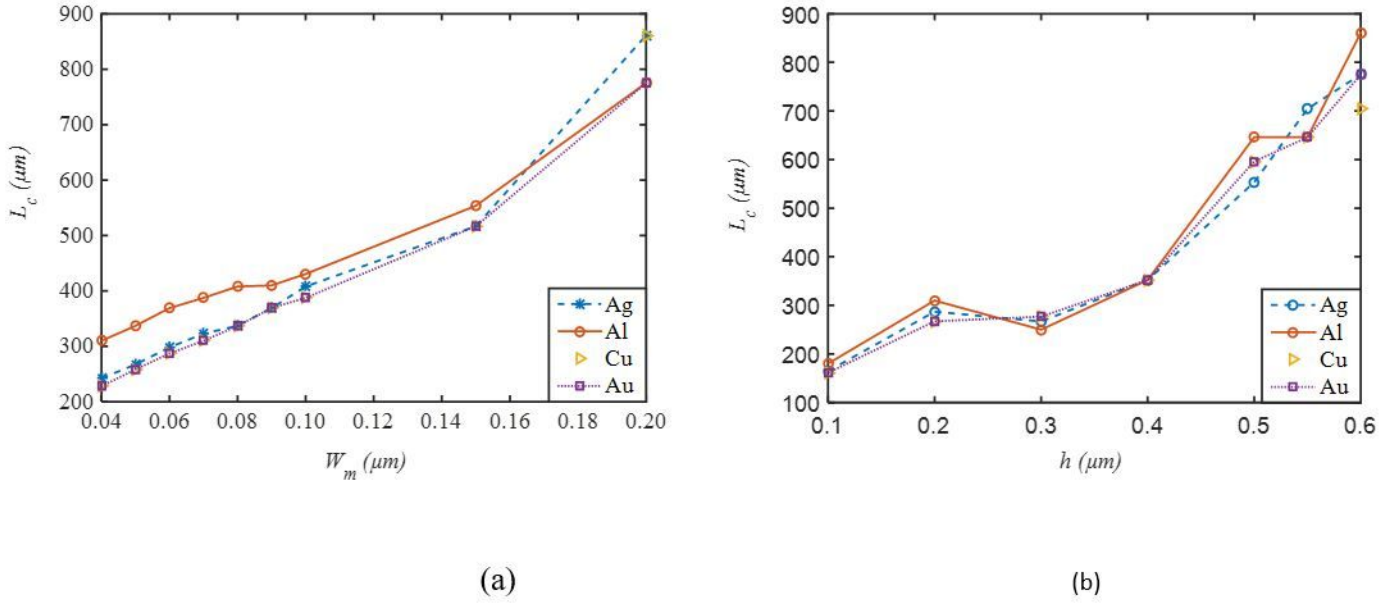

Figure 13

Variations in coupling length vs. (a) Width (b) Height of inserted metallic strip at the centre between two HIMIPW.